Numerical Modelling of the Forging Process of Rolls for Rolling Mills

CASTAGNE*, CHARLES*, HABRAKEN*, ZHANG*, GASPARD, BATAZZI****
*** MSM Department, University of Liege, bat. B52b, Grande Traverse 1,4000 Liège, Belgium.**
**** Forcast Belgium SA, rue de la Barrière 40, B4100 Seraing, Belgium.**

1 INTRODUCTION

MSM Department of Liège University and Forcast Belgium SA work together since 1996 to define a model of forging process.
The first step was to determine the mechanical behaviour as well as the recrystallisation phenomenon thanks to thermomechanical compression tests followed by microscopic investigations.
Then, the "LAGAMINE" (1) code was used to simulate the forging process. This non linear FEM code developed at MSM uses an elasto-visco-plastic law to compute thermomechanical analysis coupled with recrystallisation (2).
Firstly, two-dimensional simulations have been performed but they could not represent reality. The real solicitation state is far from plane stress, plane strain or generalized plane strain where simple assumptions define the thickness of the studied slice. So, now, three-dimensional simulations are performed.

This article presents comparisons of a forging process between two flat tools or two round tools as well as different temperatures of the roll. Simulation results help to recover and to better understand long practice in the forging industry.
A final simulation with coupling approach between thermomechanical state and recrystallisation process shows the present further investigation. The final goal is a better process optimisation, taking into account power limitation of the press and final microstructure of the roll.

2 THE NUMERICAL MODEL

2.1 The mechanical solid law

In solid elements, the stresses are computed by an elasto-visco-plastic constitutive law of Norton-Hoff type (2) with thermal effects. Its formulation is :

$$\bar{\sigma} = K_o \bar{\varepsilon}^{p4}.\exp(-p_1\bar{\varepsilon})p_2.\sqrt{3}(\sqrt{3}.\dot{\bar{\varepsilon}})^{p3} \quad (1)$$

where $\bar{\sigma}$ and $\bar{\varepsilon}$ are respectively the equivalent Cauchy stress and strain, $\dot{\bar{\varepsilon}}$ the equivalent strain rate and K_0, p_1, p_2, p_3, p_4 are material parameters. The deviatoric visco-plastic strain rate $\hat{\varepsilon}_{ij}^{vp}$ gives the tensorial form of this law :

$$\hat{\dot{\varepsilon}}_{ij}^{vp} = \frac{(J_2)^{\frac{1-p_3}{2p_3}}.\bar{\varepsilon}^{\frac{-p_4}{p_3}}.\exp(\frac{p_1}{p_3}\bar{\varepsilon}).\hat{\sigma}_{ij}}{2.(K_o p_2)^{1/p_3}} \quad (2)$$

where $\hat{\sigma}_{ij}$ is the deviatoric stress tensor and $J_2 = \frac{1}{2}\hat{\sigma}_{ij}\hat{\sigma}_{ij}$ the second stress invariant. Such description allows the modelization of a behaviour which includes hardening and softening.
The thermal dependence of the parameters p_1 to p_4 is defined by :

$$p_4 = \text{constant} \qquad p_3 = \text{constant}$$
$$p_1 = -\left(\frac{T}{C_1}\right)^{C_2} + C_3 \qquad p_2 = \left(\frac{C_4}{T}\right)^2 + \frac{C_5}{T} + C_6 \quad (3)$$

where T is the temperature and C_1, C_2, C_3, C_4, C_5, C_6 are material constants.

The integration is computed by an implicit method :

$$\hat{\dot{\sigma}}_{ij} = 2G\left(\hat{\dot{\varepsilon}}_{ij}^{total} - \hat{\dot{\varepsilon}}_{ij}^{vp}\right) + \frac{1}{G}\frac{\partial G}{\partial T}\hat{\sigma}_{ij}\dot{T} \text{ or } \underline{\hat{\dot{\sigma}}}(t) = h(\underline{\hat{\sigma}}, \bar{\varepsilon}, T) + g(t, T) \quad (4)$$

where t is the time and the second order tensors are either expressed by their indicial notation or underlined.
If we suppose that we known $\underline{\hat{\sigma}}_k$ at time $t = t_o$, the difficulty is to compute $\underline{\hat{\sigma}}_{k+1}$ at time $t = t_o+\Delta t$. Developing the equation (4) in a Taylor series of first order, we found the expression giving the variation of the deviatoric stress tensor:

$$\left[\underline{\underline{I}} - \left.\frac{\partial h}{\partial \underline{\hat{\sigma}}}\right|_{t_o}.\theta.\Delta t\right]\Delta\underline{\hat{\sigma}} = \Delta t.\left[h\left[\underline{\hat{\sigma}}_k, \bar{\varepsilon}_k, T(t_o)\right] + \underline{g}(t_o + \theta\Delta t, T(t_o))\right] + \theta.\Delta t\left[\left.\frac{\partial h}{\partial \bar{\varepsilon}}\right|_{t_o}\Delta\bar{\varepsilon} + \left.\frac{\partial h}{\partial T}\right|_{t_o}\Delta T + \left.\frac{\partial g}{\partial T}\right|_{t_o}\Delta T\right] \quad (5)$$

with $0<\theta<1$. Generally we use $\theta = 2/3$.

2.2 Computation of the dynamic recrystallised fraction (partial uncoupled approach)
The implemented model is based on the work of Sellars and Kopp (3, 4, 5).
The curves $\varepsilon_C(Z)$ and $\varepsilon_S(Z)$ respectively express the limit strains for the recrystallisation beginning and end versus Zener parameter.

This parameter is a function of the strain rate $\dot{\bar{\varepsilon}}$, the activation energy Q, the temperature T and the Boltzman constant R :

$$Z = \dot{\varepsilon} \exp\left(-\frac{Q}{RT}\right) \tag{6}$$

Experimentally defined, each curve, $\varepsilon_C(Z)$ or $\varepsilon_S(Z)$, is expressed by an analytical function depending on 4 materials parameters R_1 to R_4.

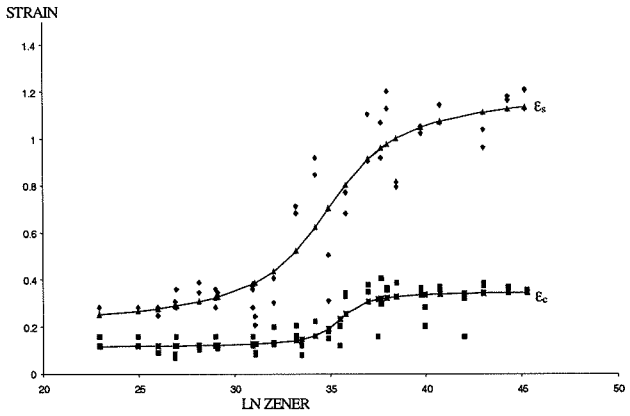

Figure 1 : Example of curves defining the beginning and the end of the recrystallisation

$$\varepsilon_{C/S} = R_1 * \mathrm{ATAN}[(\ln(Z) - R_2) * R_3] + R_4 \tag{7}$$

If Zener parameter is constant, the recrystallised fraction X_{dyn} is obtained by an Avrami law. This law is largely used to represent kinetics of metallurgical transformations. We found it as well for phase transformations (austenitic, perlitic...) as to modelize the static or dynamic recrystallisation. Its general form is:

$$X = 1 - \exp(-b\, t^n) \tag{8}$$

where X is the recrystallised fraction, here t is the time from the recrystallisation beginning and b, n are material constants.

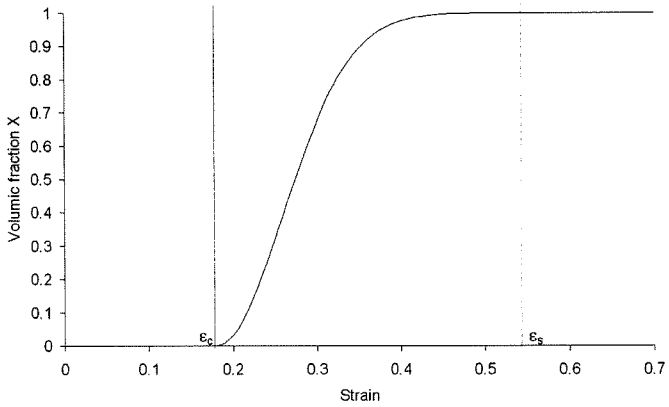

Figure 2 : The Avrami law.

We consider that the structure is completely recrystallised if the volume fraction value of 95% is reached. So the Avrami law can be written as :

$$X = 1 - EXP\left[-3 * \left(\frac{\varepsilon - \varepsilon_c}{\varepsilon_s - \varepsilon_c} \right)^n \right] \tag{9}$$

Based on Avrami approach, our computational algorithm is described hereafter, it takes into account the variation of Zener parameter during the real recrystallisation process.

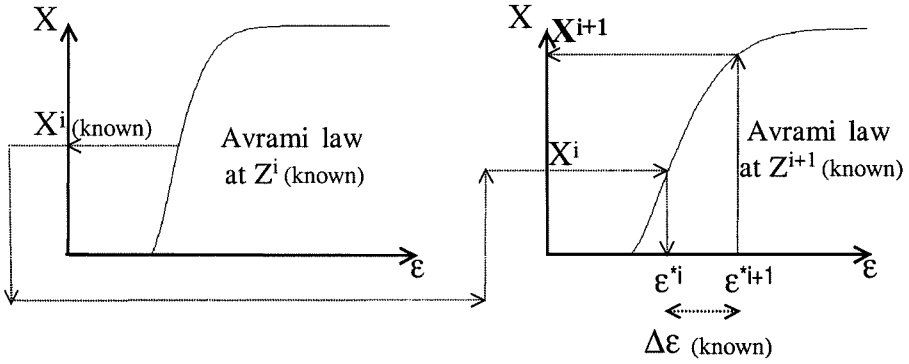

Let us use the subscript i to define the configuration at the beginning of the step and subscript i+1 to define the configuration at the end of the step.

The recrystallised fraction X^i is known and was computed during the previous step. This value is reported in the Avrami law at time i+1 and a fictive strain ε^{*i} is computed. Knowing the strain increment on the step i - i+1, we can compute the new recristallized fraction X^{i+1} according to the Avrami law at time i+1 by using equation 9.

The recrystallised fraction for the step i,i+1 is equal to the difference between the recrystallised fraction computed at the end of the step and the one computed at the previous step.

$$DX_{dyn} = X_{dyn}^{i+1} - X_{dyn}^{i} \tag{10}$$

The total recrystallised fraction is equal to the addition of the recrystallised fractions computed at each step, since the beginning of the simulation.

$$X_{dyn}^{i+1} = \left(1 - X_{dyn}^{i}\right) * DX_{dyn} + X_{dyn}^{i} \tag{11}$$

This method is additive; the microstructure is directly coupled from the thermal and mechanical history of the material. However in this partially uncoupled approach, the recrystallisation process does not affect the thermal and mechanical properties.

2.3 The total coupling case

The principle is that each integration point of the mesh is divided into substructures defined by their volumic fraction A and their hardening degree directly related to the recrystallisation process and the macroscopic strain. Each substructure follows one microscopic stress curve $\underline{\sigma}_{micro}$ ($\underline{\varepsilon}_{micro}$). At the substructure birth, $\underline{\varepsilon}_{micro}$ is assumed to be zero, then it increases with macroscopic strain rate $\underline{\dot{\varepsilon}}$. So $\underline{\varepsilon}_{micro}$ plays more the role of a hardening variable than a real strain.

During one time step, at each integration point of the mesh, the FEM code loops over the substructures defining this integration point and actualises, for each substructure, the stresses, the strains and the Zener parameter. It also checks if the recrystallisation is in progress or not, which induces death, birth or volume change of some substructures.

So, for one substructure, four cases are possible:

- the equivalent strain is lower then ε_c : no recrystallisation, the volumic fraction of the substructure is unchanged;
- the recrystallisation occurs but it is the beginning: the phenomena is neglected because the recrystallised fraction A is smaller then the minimum fraction A_{min};
- the recrystallisation occurs and is quasi completed: the old substructure disappears and a new substructure is created;
- the recrystallisation occurs and is partial: the old substructure is kept and its volume is actualised and a new substructure is created.

At the end of the substructures loop, the macroscopic stresses are computed according to the stresses of the substructures by a mixing law.

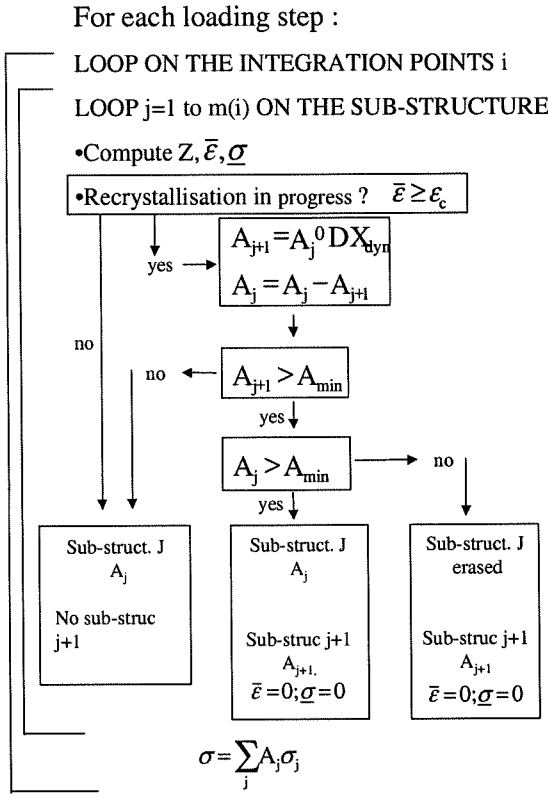

3 HOT COMPRESSION TEST

Hot compression tests on small cylinders at different temperatures and strain rates are made till strain level from 0.1 up to 0.7. The temperature is regulated by using K type thermocouples and the heating is performed by using a quad elliptic chamber with four

infrared lamps. The temperature and the strain rate $\dot{\varepsilon}$ are kept constant during the compression test thanks to regulation (see figure 3).

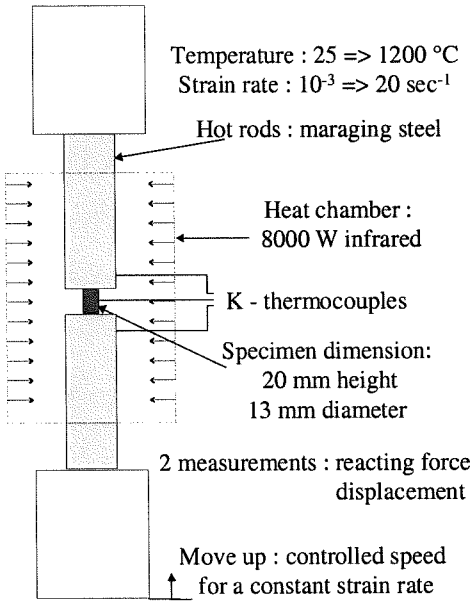

Figure 3 : Hot compression test description.

Thanks to these hot compression tests, we are able to characterise the mechanical behaviour of the tested forging steel. The following figure shows the obtained true stress – true strain curves.

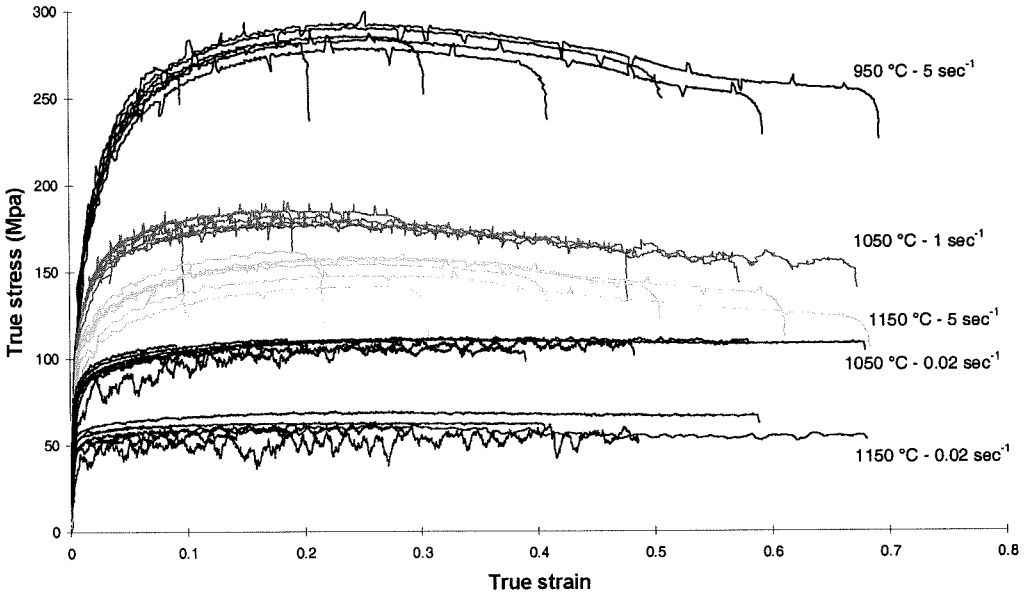

Figure 4 : True stress – true strain curves of a forging steel.

A metallographic study of the quenched cylinders gives the recrystallised fraction function of the strain, the strain rate and the temperature. This study is still in progress, so the following figure does not represent the final results.

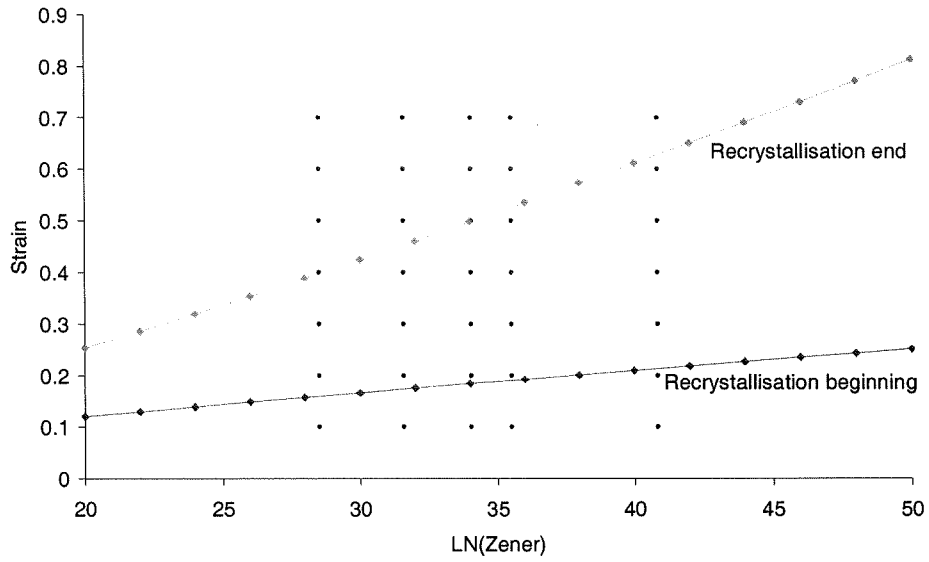

Figure 5 : Recrystallisation according to the strain, the strain rate and the temperature

4 SIMULATIONS

First, a forging process of a roll was simulated in 2D. But the results obtained were not significant. So 3D simulations were necessary to better reproduce the reality of the phenomena as explained here under. Due to the symmetry, only a quarter of the roll is used for the mesh.

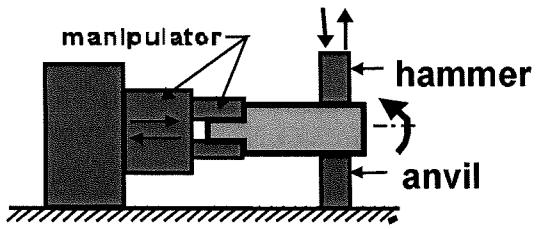

Figure 6 : The forging process

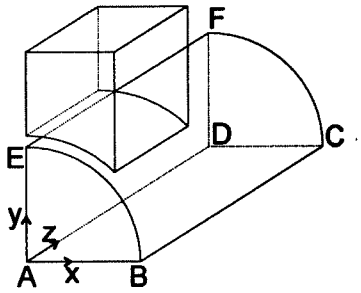

Figure 7 : The symmetry.

4.1 2D simulations

It was impossible to simulate the forging process either in plane strain state because the solicitation is not constant along the roll or in plane stress state because of the length of the roll. So we tried to use a generalised plane state to simulate the process.

A slice of roll, the thickness of which is constant in space but variable in time is simulated. All the forces that are perpendicular to the roll are balanced at the level of one degree of freedom connected to the roll thickness which is constant for all the elements. These forces come from the mechanical stress field in the solid. But, in practice, the experience shows that the thickness of the roll varies in space. In fact, the centre of the roll is more deformed than its skin which is cooler and participates at the hardness of the tools. So, it was necessary to perform 3D simulations.

4.2 3D simulations

In 3D simulations, we have compared the influence of the tools shape and of the initial temperature of the forged roll. If there is a cooling of the skin before forging, it participates with the tool during the forging process and the centre of the roll is more deformed, which is better. But if the cooling time is too long, the cooling benefice disappears as we see in the following results.

4 cases were simulated: the applied force is the same in each case and its maximum is equal to $4\ 10^7$ N.

- Flat tools – no cooling : the temperature is 1423 K (1150 °C) and constant in time and space;
- Round tools - no cooling : the temperature is 1423 K (1150 °C) and constant in time and space;
- Round tools - a cooling of 20 min : the initial temperature is 1423 K (1150 °C), then a thermal simulation models a 20 min cooling. The final temperature varies form 1134 (861 °C) to 1423 K (1150 °C) and is kept constant during the simulation of forging;
- Round tools - a cooling of 80 min : the initial temperature is 1423 K (1150 °C), then a thermal simulation models a 80 min cooling. The final temperature varies form 1002 (729 °C) to 1419 K (1146 °C) and is kept constant during the simulation of forging.

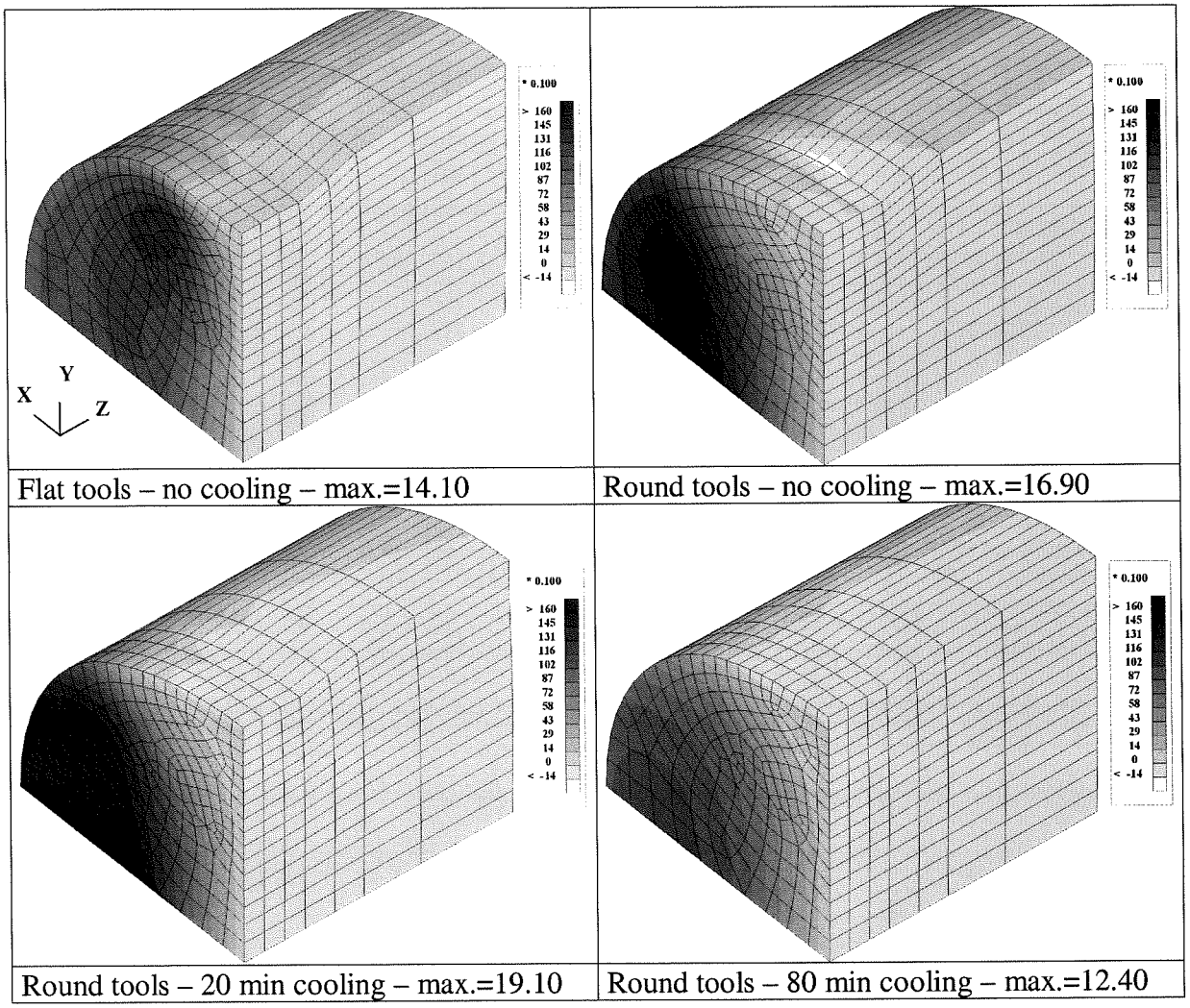

Figure 8 : Displacement along x (mm)

The displacements along the x and the z axis show that it is better to use round tools then flat ones because the displacements are concentrated more in the centre of the roll and their maximum values are bigger.
Now, we compare the results obtained for round tools and for several cooling times. We can see on figures 8 and 9 that a too long cooling time is not recommended as the roll can not be forged anymore because of its too low temperature. A 20 min. cooling time seems to be better to obtain the maximum displacements along the x axis. However, looking to the z axis displacements, the gain it less.

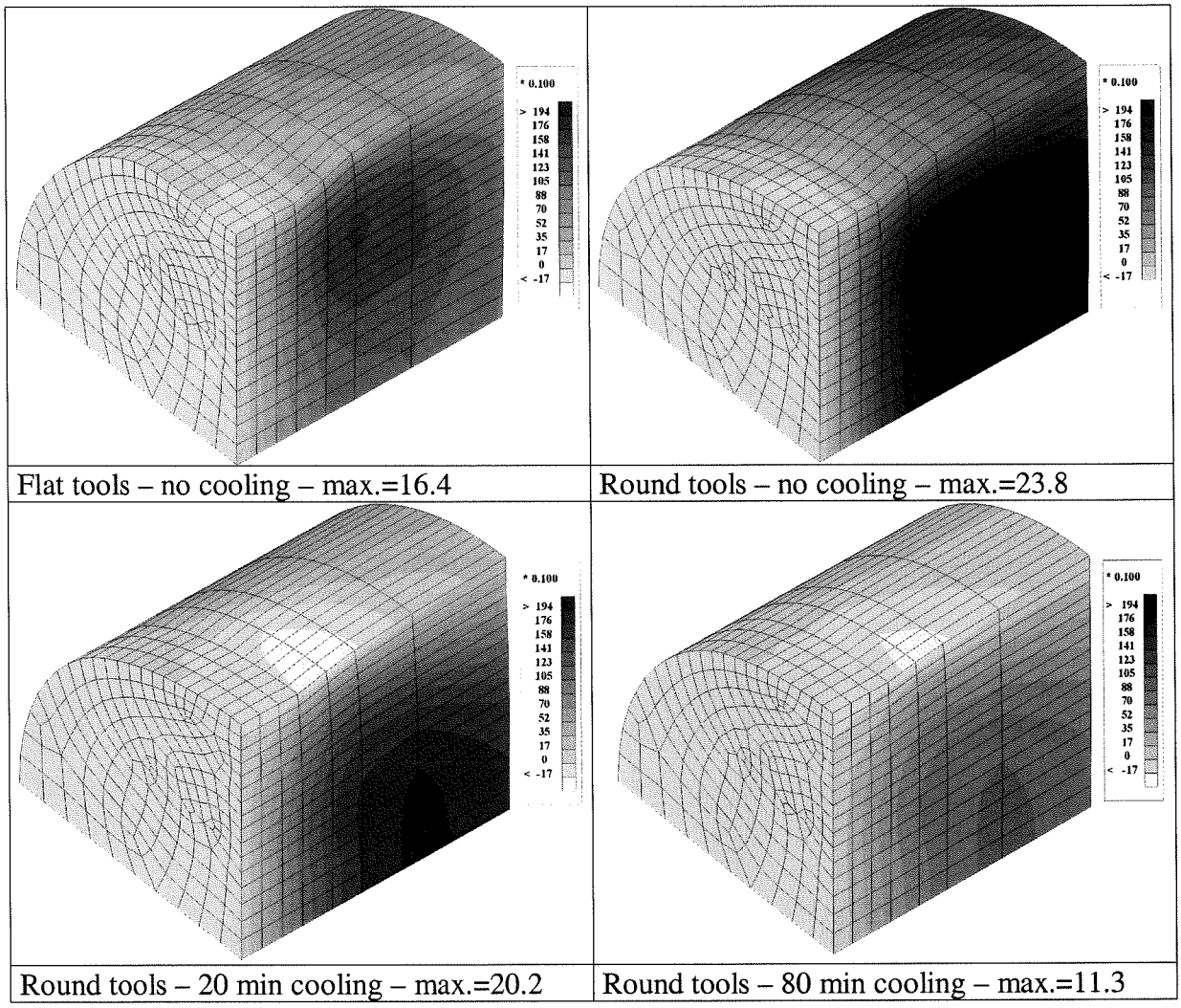

Flat tools – no cooling – max.=16.4 | Round tools – no cooling – max.=23.8

Round tools – 20 min cooling – max.=20.2 | Round tools – 80 min cooling – max.=11.3

Figure 9 : Displacement along z (mm)

4.3 3D simulations with coupled recrystallisation

For this simulation, we use the same data as the case 2 (round tools – no cooling) except we have a coupling between the thermomechanical analysis and the recrystallisation. As the recrystallisation parameters identification is still in progress, the presented results are just qualitative. The displacement distributions along the x and the z axis are quite comparable with those obtained by the simulation without recrystallisation. If we have a look on figure 10 which represents the recrystallised volumic fraction, we see that there are two maximum recrystallisation zones. The first one is located under the skin of the roll where is located the

end of the round tools. The second one is located in the centre of the roll where the temperature is maximum.

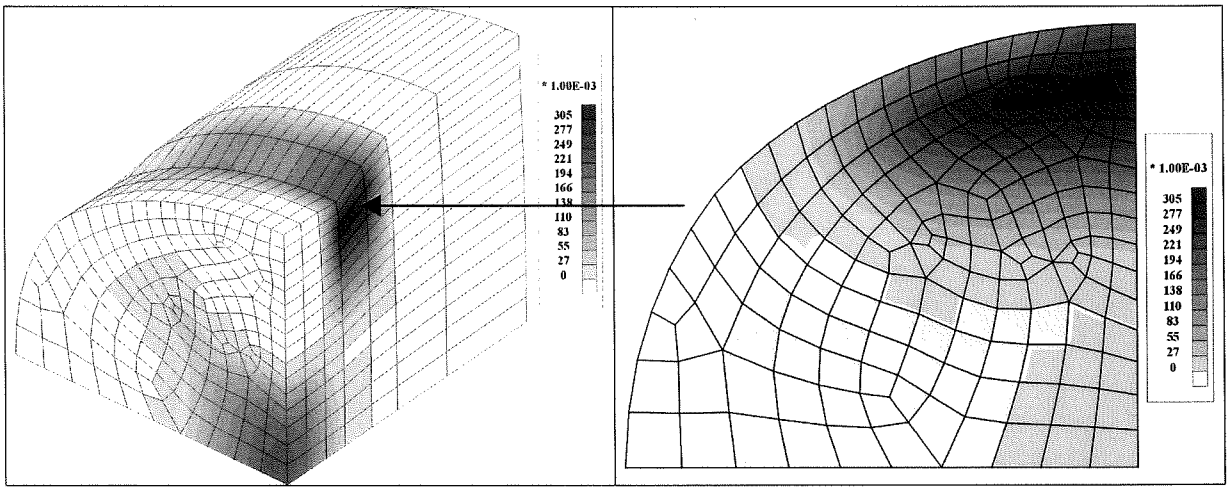

Figure 10 : Recrystallised volumic fraction

5 CONCLUSION

The described elasto-visco-plastic model is able to simulate forging process of rolls. The simulations show the importance of the tools shape on the results as well as the importance of the cooling time elapsed before the forging process. For a short cooling time, the skin of the roll participates with the tools in the forging process which is benefit but, if the cooling time is too long, this benefit disappears due to the too low initial temperatures.
The computation of the dynamic recrystallised volumic fraction is also possible but need a long experimental campaign to accurately identify the parameters of the model.

6 ACKNOLEDGMENT

The authors are pleased to acknowledge the support of their work provided by the Région Wallone and Forcast Belgium SA

7 REFERENCES

(1) S. Cescotto, A.-M. Habraken, J.-P. Radu, R. Charlier, "Some recent developments in computer simulation of metal forming process", Proc. of the 9th. Intnl. Conf. On Computer Methods in Mechanics, Vol. 4, 16-20 May 1989, Krakow, Poland.
(2) A.-M. Habraken, J.-F. Charles, J. Wegria, S. Cescotto, "Dynamic recrystallisation during Zinc Rolling", First issue of Int. J. of Forming Processes, 1997
(3) Sellars, Acta. Met. 17, pp1033/43 ,1969
(4) Kopp, R & Karhausen, K, "Application of FEM and elementary theory of plasticity to prediction of microstructure in hot rolling", 1st Intnl. Conference on Modeling of Metal Rolling Processes, 1993, Imperial College
(5) Kopp, R. & Karhausen, K., "Model for Integrated Process and Microstructure Simulation in Hot Forming", Jnl. Of Constructional Steel Research, Vol. 63, n°6, pp. 247-256, 1992